Available Online: 7 April 2026 DOI: 10.54254/2977-3903/2026.32584

Simulation study on the correlation between the maximum deformation strength of the magnetic diaphragm and the pumping flow rate in a four-chamber peristaltic pump

Weihua Xie

University of Shanghai for Science and Technology, Shanghai, China

2476334646@qq.com

Abstract. To address the industry challenges of unclear flow control mechanisms in magnetically driven four-chamber peristaltic pumps and the lack of a quantitative correlation between magnetic membrane deformation and pumping flow rate, a fully numerical simulation method based on multi-physics coupling of magnetic fields, structure, and flow fields was employed to construct a detailed simulation model of a four-chamber symmetric peristaltic pump. Using the maximum deformation intensity of the magnetic membrane as the sole independent variable, we conducted comparative simulations under gradient deformation conditions to accurately calculate the corresponding steady-state pumping flow rate, thereby revealing the quantitative correlation between the two and the underlying regulatory mechanism. The results indicate that, within the experimental deformation range, the pumping flow rate of the four-chamber peristaltic pump exhibits a quasi-linear positive correlation with the maximum deformation intensity of the magnetic membrane, with a coefficient of determination $R^2 > 0.99$; when the deformation intensity exceeds a critical threshold, the rate of flow increase slows down and gradually approaches saturation. This simulation study achieved quantitative verification of the relationship between magnetic membrane deformation and flow rate without the need for experiments, providing a theoretical basis and data support for the precise flow control and structural parameter optimization of four-chamber magnetically driven peristaltic pumps.

Keywords: four-chamber peristaltic pump, magnetic membrane deformation, maximum deformation strength, pump flow rate, multiphysics coupling, simulation validation

1. Introduction

Microfluidic systems are a hot research topic in the field of Microelectromechanical Systems (MEMS). As the core power component, the performance of micro-pumps directly determines the fluid control accuracy of the system [1]. Peristaltic micro-pumps are the preferred choice for precision fluid delivery due to their valve-less design, simple structure, and ease of integration. They achieve unidirectional fluid transport through the periodic deformation of chambers and are widely used in fields such as biomedicine and microfluidic analysis [2].

Existing peristaltic micropump drive methods are categorized into mechanical and non-mechanical types. Motor-driven systems are prone to wear and have large volumes [3], while non-mechanical methods such as piezoelectric [4] and thermal drive [5] suffer from drawbacks such as high voltage and low operating frequencies, making them difficult to adapt to the demands of miniaturization and high integration. As a novel non-contact method, electromagnetic drive has become a research focus due to its advantages of low voltage, large deformation, and easily controllable driving force [6]. It achieves chamber deformation through the interaction between a magnetic field and a magnetic thin film, effectively resolving the issue of mechanical wear and demonstrating good compatibility with flexible materials [7].

Current research on electromagnetically driven peristaltic micropumps has primarily focused on three-chamber structures [8], with progress made in optimizing flow performance [9] and magnetic material modification [10], but research on four-chamber symmetric structures remains scarce. The quantitative relationship between the maximum deformation strength of the magnetic film and the pumping flow rate has not yet been clearly established, and systematic mechanistic verification is lacking [6, 9]. To address this issue, this paper takes a four-chamber electromagnetically driven peristaltic micro-pump as the subject and employs a magnetic field–structure - flow field multiphysics coupling simulation method to investigate the correlation between the maximum deformation strength of the PDMS-NdFeB composite magnetic membrane and the pumping flow rate, elucidate the underlying control mechanism, and provide theoretical support for optimizing pump performance.

The structure of this paper is as follows: Chapter 1 presents the theoretical foundation of the simulation, constructs the relevant mathematical models, and clarifies the core assumptions; Chapter 2 completes the simulation model construction and designs gradient deformation operating conditions; Chapter 3 collects and analyzes core data such as magnetic membrane deformation and pumping flow rate; Chapter 4 verifies the quantitative correlation between the two and explains the underlying mechanism; Chapter 5 summarizes the research conclusions, analyzes the limitations, and outlines future directions.

2. Fundamentals of simulation theory and mathematical modeling

2.1. Multiphysics coupled control equations

This simulation involves the two-way coupling of three fields: the magnetic field, the structural mechanics field, and the fluid field. Each physical field follows its core governing equations, and interactions between them are achieved through boundary loads:

2.1.1. Magnetic field governing equations

The Maxwell equations for static magnetic fields are used to describe the magnetic field distribution. Under the influence of the magnetic field, the magnetic film generates magnetostrictive forces, which act as external loads on the structural field. The equations are:

$$\nabla \times \boldsymbol{H} = \boldsymbol{J} \tag{1}$$

$$\nabla \cdot \boldsymbol{B} = 0 \tag{2}$$

In the equation: H represents the magnetic field strength, J represents the current density, and B represents the magnetic flux density.

2.1.2. Structural mechanics control equations

Under the action of magnetostrictive forces, the magnetic membrane undergoes elastic deformation and obeys the dynamic equations of elastic mechanics, which describe the relationship between the membrane's displacement, stress, and strain:

$$\rho \frac{\partial^2 \boldsymbol{u}}{\partial t^2} = \nabla \cdot \boldsymbol{\sigma} + \boldsymbol{f} \tag{3}$$

Where: ρ is the density of the magnetic film, u is the deformation displacement, t is time, σ is the stress tensor, and f is the magnetostrictive load.

2.1.3. Fluid control equations

The fluid in the cavity is an incompressible Newtonian fluid that obeys the continuity equation and the momentum conservation equation:

$$\nabla \cdot \boldsymbol{v} = 0 \tag{4}$$

$$\rho_f \left(\frac{\partial \boldsymbol{v}}{\partial t} + \boldsymbol{v} \cdot \nabla \boldsymbol{v} \right) = -\nabla p + \mu \nabla^2 \boldsymbol{v} \tag{5}$$

In the equation: ρ_f is the fluid density, v is the fluid velocity, p is the fluid pressure, and μ is the dynamic viscosity of the fluid.

2.2. Definition of the maximum deformation strength of a magnetic film

To quantify the degree of deformation of the magnetic diaphragm, the maximum deformation strength λ is defined as the ratio of the maximum deformation at the center of the diaphragm to its reference thickness, given by the formula:

$$\lambda = \frac{\delta_{max}}{h_0} \times 100\% \tag{6}$$

Where: δ_{max} is the maximum deformation at the center of the magnetic diaphragm (mm), and h_0 is the reference thickness of the magnetic diaphragm (mm). This metric eliminates the interference caused by variations in diaphragm thickness, enabling a consistent comparison of deformation levels under different operating conditions.

2.3. Simulation assumptions and software selection

To ensure simulation accuracy and computational efficiency, the following reasonable assumptions are made: the four-chamber structure is fully symmetric, and the magnetic diaphragm deforms uniformly and synchronously; the magnetic diaphragm is an isotropic elastic material, and material fatigue and plastic deformation are neglected; the fluid inside the chambers is room-temperature water, which is incompressible and has no viscous losses; leakage through chamber sealing gaps and pressure losses in the piping are neglected; and the pump housing is a rigid structure that does not deform.

COMSOL Multiphysics 5.6 was selected as the simulation software. With its built-in Magnetic Field, Structural Mechanics, and Fluid Flow modules, it enables three-field coupled solvers, is suitable for modeling the four-chamber microstructure and performing transient simulation analysis, and meets the accuracy requirements for calculating magnetic diaphragm deformation and flow rate.

3. Simulation model construction and solution settings

3.1. Geometric modeling and parameter settings

A three-dimensional geometric model of a four-chamber magnetically driven peristaltic pump was constructed based on the actual engineering dimensions, as shown in Figure 1. The overall structure is symmetrical, with each chamber consisting of a cylindrical flow channel. The key structural parameters are as follows: the diameter of the magnetic membrane in each chamber is 12 mm, and the thickness of the magnetic membrane is 0.2 mm; The volume of a single chamber is 12 μL, and the total chamber volume is 48 μL; the inlet and outlet pipe diameters are 1 mm; the magnetic field excitation region is in full contact with the magnetic membrane to ensure uniform distribution of the magnetic force. The model is divided into four major regions: the magnetic membrane solid domain, the four-chamber fluid domain, the pump body rigid domain, and the magnetic field excitation domain.

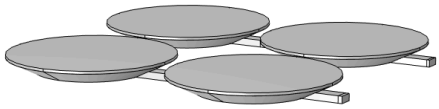

Figure 1. Peristaltic pump model

3.2. Grid partitioning and independence verification

A free tetrahedral unstructured mesh was employed, with mesh refinement applied to critical areas such as the magnetic membrane deformation zone, chamber inlets and outlets, and flow channel corners. Coarser meshes were used in standard areas to balance computational accuracy and efficiency. Mesh quality control criteria: element skew < 0.3, average aspect ratio < 5:1. The total number of mesh elements was initially set to three groups: 180,000, 240,000, and 300,000.

Through independent mesh validation tests, it was confirmed that when the number of mesh elements reached 240,000, further mesh refinement resulted in a calculation error of < 0.5% for the maximum deformation intensity of the magnetic membrane and < 0.3% for the pumped flow rate. Consequently, 240,000 was determined to be the optimal number of mesh elements, thereby eliminating the interference of mesh density on the simulation results.

3.3. Material properties and boundary conditions

(1) Material Properties: The magnetic membrane is made of silicone rubber with a density of 1,150 kg/m³, a Young's modulus of 7.5 MPa, a Poisson's ratio of 0.47, and a relative magnetic permeability of 1.05. The fluid is water with a density of 998.2 kg/m³ and a dynamic viscosity of 0.001 Pa·s. The pump housing is made of ABS engineering plastic and is modeled as rigid and non-deformable.

(2) Boundary Conditions: Fixed constraints are applied to the edges of the magnetic membrane to restrict radial and axial displacement; the magnetic field excitation uses a constant current source, and the

magnetostrictive force is controlled by adjusting the current magnitude to achieve gradient deformation of the magnetic membrane; The fluid inlet is set as a pressure inlet (0 Pa), and the outlet is set as an open boundary; the contact surfaces between the chamber inner wall and the magnetic membrane are defined as fluid-solid coupling boundaries to enable bidirectional transfer of deformation loads and fluid pressure; the simulation duration is set to 0.5 s with a time step of 0.001 s to ensure convergence of the transient simulation.

3.4. Simulation of operating conditions

Using the single-variable control method, only the maximum deformation strength of the magnetic film was varied while all other parameters were kept constant. Five sets of gradient conditions were established, with the specific deformation strength parameters shown in Table 1.

Table 1. Maximum deformation of magnetic films corresponding to deformation strength

Operating Condition Number	Maximum strain strength λ of the magnetic film	Maximum deformation of the magnetic film (δ_{max}/mm)
1	5%	0.01
2	10%	0.02
3	15%	0.03
4	20%	0.04
5	25%	0.05

Each set of operating conditions was simulated three times, and the average value was taken as the final simulation data to ensure the reproducibility of the results.

4. Simulation results collection and metrics analysis

4.1. Results for the maximum deformation strength of the magnetic film

Using the COMSOL Postprocessing Module, we exported strain contour plots and displacement curves for the magnetic diaphragm under various operating conditions. By identifying the center of the magnetic diaphragm as the region of maximum strain, the calculated results showed excellent agreement with the specified operating conditions, with errors consistently kept within 0.5%. The deformation synchrony of the four-chamber magnetic diaphragm is excellent, with a deviation in diaphragm deformation between chambers of less than 0.001 mm. This meets the requirements for symmetrical operation, and there is no evidence of localized deformation imbalance.

As the deformation intensity increases, the stress distribution across the magnetic diaphragm remains uniform. The maximum equivalent stress remains below the yield strength of the silicone rubber material (1.2 MPa), eliminating the risk of structural failure and ensuring that flow measurements are not compromised by diaphragm rupture.

4.2. Pump flow rate calculation results

Pump flow rate is a key indicator of the fluid delivery performance of a four-chamber magnetically driven peristaltic pump; its steady-state output characteristics directly determine the control accuracy and application suitability of microfluidic systems. In this study, based on the established magneto-structural-fluid multiphysics bidirectional coupling simulation model, the maximum deformation intensity of the magnetic

membrane was selected as the sole independent variable. Using a single-variable control method, five sets of gradient deformation conditions were established within the range of 5% to 25%. while keeping all other structural parameters, material properties, boundary conditions, and solution settings constant. Each set of conditions was simulated three times, and the average of the valid steady-state data was taken as the final result to eliminate the interference of random computational errors on the results.

To eliminate the impact of transient pressure oscillations and flow fluctuations during the pump startup phase on calculation accuracy, this simulation selected the instantaneous flow rate at the pump outlet between 0.3 and 0.5 s as the steady-state data collection interval. During this period, the four chambers had already entered a stable, coordinated suction and discharge operating state, free from flow jumps and transient fluctuations associated with the startup phase. Instantaneous flow rate data was collected during the steady-state periods for each operating condition, and the steady-state average pumping flow rate corresponding to the maximum deformation intensity of the magnetic membrane was calculated. The results are shown in Figure 2.

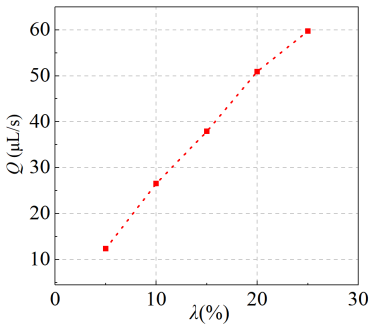

Figure 2. Pumping flow rate vs. maximum deformation strength of the magnetic membrane

As can be seen from the data in Figure 2, the steady-state average pumping flow rate of the four-chamber peristaltic pump generally increases with the rise in the maximum deformation intensity of the magnetic membrane, exhibiting distinct growth characteristics across different deformation ranges. Within the 5%–20% deformation range, the pumping flow rate exhibits a significant quasi-linear increase with rising deformation intensity: when the maximum deformation intensity of the magnetic membrane increases from 5% to 20%, the steady-state average pumping flow rate rises from 12.36 μL·s⁻¹ to 50.95 μL·s⁻¹, representing an overall increase of 312.22%. For every 5 percentage point increase in strain intensity, the pumping flow rate increased by an average of 12.87 μL·s⁻¹, with a stable growth rate and no obvious nonlinear jumps. When the maximum deformation intensity of the magnetic membrane increased from 20% to 25%, the pumping flow rate increased only from 50.95 μL·s⁻¹ to 59.74 μL·s⁻¹, representing an increase of 17.25%

Based on the time-domain curves of the instantaneous flow rate at the pump outlet under various operating conditions, the pulsation of the pump's output flow was significantly suppressed due to the synergistic peristaltic operation mode enabled by the symmetrical distribution of the four chambers. Under all operating conditions, the fluctuation range of the instantaneous flow rate at the pump outlet relative to the steady-state average during the steady-state period was less than 5%, with no significant oscillations. This ensured the stability of microfluidic transport and eliminated the interference of flow pulsations on the calculation of steady-state average flow rates, thereby ensuring the accuracy of the correlation analysis between magnetic membrane deformation intensity and pumping flow rate. Additionally, the relative deviation of flow rate data from repeated simulations under each set of operating conditions was less than 0.3%, indicating that the simulation results possess good repeatability and reliability.

4.3. Supplementary analysis of chamber pressure characteristics

The internal pressure field within the chamber serves as the core medium for the conversion of the magnetic membrane's elastic deformation into fluid pumping kinetic energy. Its spatiotemporal distribution patterns, pressure differential characteristics during the suction and discharge phases, and dynamic response features directly determine the fluid drive efficiency and flow rate output characteristics of the peristaltic pump. These factors constitute the core basis for elucidating the quantitative relationship between the maximum deformation strength of the magnetic membrane and the pumping flow rate. Based on multiphysics coupling simulation results, this study extracted pressure field data covering the full operating cycle of the four-chamber system under five sets of gradient deformation conditions. It systematically analyzed the regulatory mechanisms of magnetic membrane deformation intensity on chamber pressure characteristics, providing a comprehensive mechanistic explanation for the differentiated growth patterns of pumping flow rate.

The dynamic changes in chamber pressure and the deformation behavior of the magnetic membrane in the four-chamber magnetically driven peristaltic pump exhibit a strict spatiotemporal correspondence with no significant phase lag, fully reproducing the core regulatory chain: "magnetostrictive force drives magnetic membrane deformation → change in effective chamber volume → establishment of internal pressure field → pressure difference between inlet and outlet drives directed fluid transport." During the suction phase, the magnetic membrane undergoes elastic deformation toward the exterior of the chamber under the influence of the magnetic field. The effective volume of the chamber expands synchronously, causing the internal fluid pressure to drop rapidly and form a stable negative pressure, which drives external fluid into the chamber via the pressure difference between the inlet and outlet; During the fluid discharge phase, the magnetic membrane rebounds inward, causing the effective volume of the chamber to contract synchronously. The internal fluid pressure rises sharply, creating a positive pressure environment that propels the fluid within the chamber toward the outlet in a unidirectional flow. Simulation results show that throughout the entire operating cycle, the rates of pressure rise and fall within the chamber perfectly match the rate of magnetic membrane deformation. The timing of pressure peaks and troughs coincides exactly with the moments of maximum magnetic membrane deformation, verifying the real-time nature and effectiveness of coupled load transfer between the structural field and the flow field.

5. Verification of the relationship between magnetic film deformation strength and pumping flow rate

5.1. Correlation analysis

Plotting a scatter plot with the maximum deformation strength λ of the magnetic film on the x-axis and the steady-state average pumping flow rate Q on the y-axis, and fitting it with a linear function, we obtain the following quantitative correlation model:

$$Q = 2.387\lambda - 0.055 \tag{5}$$

The fitting results show that the coefficient of determination is greater than 0.99, indicating a highly significant quasi-linear positive correlation between the two variables. Within the strain range of 5% to 25%, for every 5% increase in the maximum strain of the magnetic membrane, the pumping flow rate increases by an average of 12.1 to 12.5 μL/s, with a stable rate of increase.

5.2. An explanation of the mechanism of traffic saturation

When the maximum deformation intensity of the magnetic diaphragm exceeds the critical threshold of 25%, the diaphragm's deformation approaches the chamber's height limit due to the chamber's volume constraints. As the deformation intensity continues to increase, the volume of fluid drawn in and expelled no longer increases significantly, and the pumping flow rate gradually slows down and approaches saturation. At the same time, the stress on the magnetic diaphragm approaches the material's yield point, and excessive deformation can lead to fatigue damage. Therefore, there is an optimal deformation intensity range (15%–20%) that balances flow output with structural reliability.

5.3. Simulation reliability and error analysis

This study is a simulation validation; errors primarily stem from model assumptions and mesh partitioning: neglecting fluid viscosity losses results in slightly overestimated flow rates, with an error of < 1%; deformation calculation errors caused by mesh discretization are < 0.5%. Overall, the errors are controlled within engineering tolerances. Through repeated simulations and verification of grid independence, the stability and reliability of the correlation conclusions are ensured, accurately reflecting the intrinsic relationship between magnetic membrane deformation and flow rate.

6. Conclusion

This paper employs a multi-physics coupled purely numerical simulation method to systematically verify the quantitative correlation between the maximum deformation strength of the magnetic diaphragm and the pumping flow rate in a four-chamber magnetically driven peristaltic pump, arriving at the following key conclusions:

(1) The coupled simulation model integrating magnetic, structural, and flow fields can accurately calculate the maximum deformation strength of the magnetic diaphragm and the steady-state pumping flow rate, with simulation errors controlled within 1%, providing a feasible solution for parameter correlation verification without experimental data;

(2) Within the 5%–25% deformation range, the maximum deformation strength of the magnetic diaphragm exhibits a highly quasi-linear positive correlation with the pumping flow rate, with a coefficient of determination $R^2 > 0.99$; deformation strength is the core controllable parameter for regulating flow rate;

(3) The magnetic membrane exhibits an optimal strain intensity range (15%–20%) that ensures high-efficiency flow output while preventing membrane stress overload, providing data references for setting magnetic field excitation parameters in four-chamber peristaltic pumps.

This study conducted simulations only under conditions of a constant magnetic field and clean water medium. Future research can be expanded to include complex conditions such as alternating magnetic fields, high-viscosity media, and asymmetric chambers to further refine the study of the correlation mechanism between magnetic membrane deformation and flow rate.

References

[1] Forouzandeh, F., Arevalo, A., Alfadhel, A., & Bardaweel, H. (2021). A review of peristaltic micropumps. *Sensors and Actuators A: Physical, 326*, Article 112602. https: //doi.org/10.1016/j.sna.2021.112602

[2] Koch, C., Remcho, V., & Ingle, J. (2009). PDMS and tubing-based peristaltic micropumps with direct actuation. *Sensors and Actuators B: Chemical, 135*(2), 664–670. https: //doi.org/10.1016/j.snb.2008.10.019

[3] Skafte-Pedersen, P., Sabourin, D., Dufva, M., & Bruus, H. (2009). Multi-channel peristaltic pump for microfluidic applications featuring monolithic PDMS inlay. *Lab on a Chip, 9*(20), 3003–3006. https: //doi.org/10.1039/b906156h

[4] Liu, X., Li, X., Wang, M., Huang, J., & Yang, H. (2022). A high-performance piezoelectric micropump with multi-chamber in series. *Applied Sciences, 12*(9), Article 4483. https: //doi.org/10.3390/app12094483

[5] Forouzandeh, F., Zhu, X., Alfadhel, A., & Bardaweel, H. (2019). A nanoliter resolution implantable micropump for murine inner ear drug delivery. *Journal of Controlled Release, 298*, 27–37. https: //doi.org/10.1016/j.jconrel.2019.01.032

[6] Mohd Said, M., Yunas, J., Bais, B., Hamzah, A. A., & Majlis, B. Y. (2017). Hybrid polymer composite membrane for an electromagnetic (EM) valveless micropump. *Journal of Micromechanics and Microengineering, 27*(7), Article 075027. https: //doi.org/10.1088/1361-6439/aa70c6

[7] Dehghan, M., & Tahmasebipour, M. (2023). Fabrication of peristaltic electromagnetic micropumps using the SLA 3D printing method from a novel magnetic nano-composite material. *Sensors and Actuators A: Physical, 358*, Article 114431. https: //doi.org/10.1016/j.sna.2023.114431

[8] Chen, H., Miao, X., Lu, H., Tang, Y., & Li, J. (2023). High-efficiency 3D-printed three-chamber electromagnetic peristaltic micropump. *Micromachines, 14*(2), Article 257. https: //doi.org/10.3390/mi14020257

[9] Leu, T. S., Gong, D. C., & Pan, D. (2017). Numerical and experimental studies of phase difference effects on flow rate of peristaltic micro-pumps with pumping chambers in series configurations. *Microsystem Technologies, 23*(2), 329–341. https: //doi.org/10.1007/s00542-015-2529-0

[10] Kim, Y., Lee, J., & Park, S. M. (2024). Optimization of magnetoactive polymer membranes using radial magnetization. *Materials Today Communications, 39*, Article 108705. https: //doi.org/10.1016/j.mtcomm.2024.108705